A Molecular View of Dynamic Responses When Mixing Poly(ethylene oxide) and Poly(methyl methacrylate)

Chunxia Chen and Janna K. Maranas*

Department of Chemical Engineering, The Pennsylvania State University, University Park, Pennsylvania 16802

Received September 26, 2008; Revised Manuscript Received January 30, 2009

ABSTRACT: We use explicit atom molecular dynamics to investigate mobility in poly(methyl methacrylate) [PMMA] when blended with 10%, 20%, and 30% weight percent poly(ethylene oxide) [PEO]. The responses to blending of main chain motion, rotation of the two methyl groups, and rotation of the entire ester side chain, which is associated with the β-relaxation, are individually assessed at temperatures well above the glass transition temperature where their characteristic times overlap. We also consider the response of main chain motion in PEO to blending with PMMA. We find three classes of behavior: methyl group rotation is not influenced by blending, ester group rotation and the main chain motion of PEO are slightly altered by the change in environment, and a substantial change in dynamics is observed for main chain motion in PMMA. The observation that the β-relaxation in PMMA changes with mixing is unusual, as this is a local motion thought to be insensitive to blending. This is discussed in light of the spatial extent of localized motion and that of mixing of the two components.

Introduction

Dynamic processes in glass forming polymers occur over a large range of temporal and spatial scales and have been investigated using a variety of techniques including NMR,[1,2] dielectric spectroscopy,[3] light[4] and neutron scattering.[5,6] These processes fall into three categories, which may be defined loosely based on the relevant spatial scales. Terminal motion reflects translational mobility of the chain as a whole, and is thus connected to spatial scales comparable to chain dimensions. Segmental motion reflects motion of a statistical segment or Kuhn length sized region of the polymer chain backbone. Although their temperature dependencies become different at low temperature,[7] both terminal and segmental motions become increasingly slow as the glass transition temperature T_g is approached, and thus are associated with the primary or α-relaxation of amorphous materials. Secondary motion reflects movement of specific local regions of the polymer repeat unit, such as reorientation of a side group or methyl group rotation, with spatial scales comparable to the size of the moving unit, which is typically smaller than the Kuhn length. These motions are not influenced by passage through the glass transition and include the β-relaxation observed in amorphous materials.

Changes in mobility when two polymers are mixed have been widely investigated over the past fifteen years. There is a marked difference in the response of primary [either terminal or segmental] and secondary relaxations to this change in environment. The primary relaxations of the blend constituents shift toward one another yet are not coincident.[8−11] At the same time, primary relaxations in miscible blends are broadened compared to those of the pure components. Theories to explain these observations are based on the idea of a local region with a composition that varies from the bulk blend composition. Differences lie in the origin of the biased local composition, which can be from chain connectivity[12−14] or from thermal concentration fluctuations.[15−19]

In contrast to the primary relaxation, secondary relaxations are insensitive to changes in environment, although exceptions exist. As an example, consider poly(vinyl methyl ether) [PVME], with secondary relaxations including the β-relaxation and methyl group rotation. When blended with polystyrene [PS], both the characteristic time and the breadth of the β-relaxation are unaffected.[8] Similarly, blending with PS does not alter rotation of the methyl group in PVME, even for blends with 80 wt % PS. [20] As an exception to this rule, although Arrighi[21] et al. observed similar behavior for methyl group rotation in PS/PVME, they report that rotation of the ester CH_3 group in poly(methyl methacrylate) [PMMA] changes when mixed with solution chlorinated polyethylene [SCPE]. Investigations that observe the response of primary and secondary relaxations to blending focus on different temperature ranges: the primary relaxation is studied above T_g, whereas secondary relaxations are studied below T_g where the primary relaxation is frozen. The latter is necessary so that the primary relaxation does not contribute to the measurement. For example, in the case of methyl group rotation using quasi-elastic neutron scattering [QENS], if the measurement is made at high temperature, the methyl group protons will reflect translation related to the segmental relaxation, and methyl group rotation. In addition, the primary and secondary processes can merge in the high temperature range, such that it is not possible to separate them. In this contribution we examine the response of primary and secondary relaxations to blending in the temperature range characteristic of high frequency experiments such as deuterium NMR and QENS. To isolate secondary relaxations at high temperature, we use molecular simulation, which can directly probe locally defined motions, separating them from the primary relaxation at any temperature.

As a target system, we choose mixtures of poly(ethylene oxide) [PEO] and PMMA. The repeat units of these two polymers are illustrated in Figure 1. We have recently compared explicit atom, united atom, and coarse-grained simulations against experimental data for both pure components,[22,23] with the result that all three provide a reasonable description. In the present case, we choose the explicit atom model because we wish to examine rotation of both methyl groups in PMMA. In a previous investigation,[24] we isolated four processes in PMMA: the segmental relaxation by following motion of backbone atoms, the β-relaxation by following motion of the ester hydrogens about a virtual C_1-C bond, and rotation of the two methyl groups by following motion of the ester hydrogens about

* Corresponding author. E-mail: jmaranas@psu.edu.

10.1021/ma802183h CCC: $40.75 © 2009 American Chemical Society
Published on Web 03/16/2009

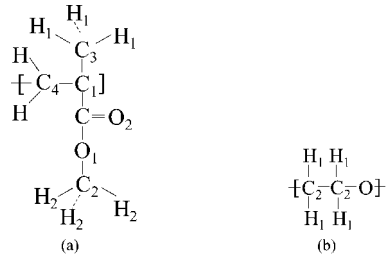

Figure 1. Repeat units of the polymers simulated: (a) PMMA and (b) PEO.

the C_2-O_1 bond or α-hydrogens about the C_1-C_3 bond. PEO exhibits a β-relaxation,[25] and an additional secondary relaxation associated with confinement.[26] The physical origin of the β-relaxation in PEO is less clear. In another polymer without side groups, it was shown that the β-relaxation is associated with the time scale of a single conformational transition, whereas the α-relaxation is associated with sampling of all conformational transitions with equilibrium probability.[27] If this is true, it is not possible to isolate the two by considering subsets of atoms, as we did for PMMA, so we consider the motion of all atoms in PEO. It has been suggested that in polymers without side groups, the β-relaxation can predominate at temperatures far above T_g, such as we consider here.[28] We assume for the time being that the primary relaxation is observed in PEO, and address the question of whether the β-relaxation contributes significantly below. We will thus follow two primary relaxations [PEO and PMMA backbone atoms], and three secondary relaxations [β-relaxation and the two methyl group rotations in PMMA] in the temperature range above the glass transition temperature of PMMA.

This blend, characterized by large T_g contrast [$\Delta T_g \sim 185$ K] and minimal interactions,[29] has been studied by dielectric spectroscopy,[30] NMR,[31] quasi-elastic neutron scattering [QENS],[32−37] and mechanical spectroscopy.[38] Of these techniques, dielectric spectroscopy targets a large frequency range and can be used above T_g to observe the primary relaxation, or below T_g to observe secondary relaxations. Observation in a mixed system depends on the dipoles present, and for the PEO/PMMA blend the β-relaxation of PMMA is strongly observed. This, combined with the fast nature of the primary relaxation of PEO, makes this process difficult to observe with dielectric measurements. PEO component dynamics have instead been investigated using NMR[13] and QENS,[35,37] which present the possibility of component labeling using deuteration, but are limited to high frequency motions and thus the temperature range above T_g. In principle, both primary and secondary relaxations would contribute with separation only possible in certain instances, for example via the spatial scale in a QENS measurement. The primary relaxation of PEO, investigated via NMR in blends with 3−30% PEO, reveals a separation from the primary relaxation of PMMA of up to twelve orders of magnitude. Relaxation times for PEO are only weakly dependent on composition,[31] suggesting a decoupling from dynamics of PMMA. Several explanations have been offered for this result: the lack of side groups in PEO leading to a decoupling of component motion,[31] observation of a secondary, rather than a primary relaxation,[28] and a relaxation times short enough to be comparable to vibration/libration[39] [the process before 1−2 ps observed in QENS on PEO and other polymers]. A common feature of all three suggestions is the extremely fast dynamics of PEO. In contrast, QENS measurements of PMMA show significant changes in the primary relaxation when mixed with PEO, with those changes consistent with the differences in T_g between pure PMMA and the blend.[32,34] Clearly, the two primary relaxations in this mixture respond quite differently, with that of PEO recently connected to confinement effects.[36] Secondary processes are invariant to environment in this system. The PMMA β-relaxation, and the PEO β- and β'-relaxations as observed at temperatures below T_g using dielectric spectroscopy remain coincident with those in the pure components.[25]

Table 1. Nonbonded Potential and Parameters for PEO−PMMA Interactions[a]

$u^{nb}(r_{ij}) = 4\varepsilon[(\sigma/r)^{12} - (\sigma/r)^6] + [1/(4\pi\varepsilon_0)][(q_i q_j)/r_{ij}]$

atom type			σ (Å)	ε (kcal/mol)	q_i (e.c.)
PMMA	C_3	C in α-CH_3 group	3.52	0.067	−0.135
	C_4	C in CH_2 group	3.52	0.067	−0.09
	C_1	main chain C group	3.20	0.051	0.00
	C	C in C=O	3.75	0.105	0.51
	O_2	O in C=O	2.96	0.210	−0.43
	O_1	ester O	3.00	0.170	−0.33
	C_2	C in ester CH_3 group	3.50	0.066	0.16
	H_1	H in alkane CH_3 or CH_2 groups	2.50	0.030	0.045
	H_2	H in ester CH_3 group	2.42	0.015	0.030
PEO	C_3	C in CH_3 group	3.88	0.095	0
	C_2	C in CH_2 group	3.88	0.095	−0.066
	O	O	3.51	0.215	−0.256
	H_1	H in CH_2 group	3.20	0.010	0.097
	H_2	H in CH_3 group	3.20	0.010	0

[a] The atom numbering corresponds to the repeat units in Figure 1.

One paper has appeared using simulation in combination with QENS to study dynamics in the PEO/PMMA blend.[36] This work focused primarily on the dynamics of PEO, specifically on the possibility of PEO being confined by the far more immobile PMMA. As such the investigated temperature range was between the blend T_g and the T_g of pure PMMA, and primary focus was on PEO mobility. In the present contribution, we focus on the temperature range above the T_g of PMMA, where both components are mobile. We investigate changes in primary and secondary relaxations, primarily of PMMA. In this sense the work is complementary to what is already available.

Simulation Details

We present explicit atom (EA) simulations on blends of PEO and PMMA at three compositions: 10%, 20%, and 30% PEO by weight. We also present EA simulations for pure PEO and pure PMMA that have been described elsewhere.[22−24] The PMMA chains have 10 repeat units and a molecular weight of 1016 g/mol, and the PEO chains have 31 repeat units and a molecular weight of 1350 g/mol. For each composition, 50 chains were placed in the simulation box, with 4, 8, and 12 PEO chains corresponding to the 10, 20, and 30 wt % blends. Simulations were run in the NVT ensemble with the volume set by the pure component densities as a function of temperature assuming no volume change on mixing, and the temperature controlled using the velocity-rescaling algorithm of Berendsen et al.[40] Simulations were carried out at seven temperatures: 400, 420, 440, 470, 500, 550, and 600 K, with the highest two temperatures for the 20% blend only. As mentioned above, the EA force fields used for pure PEO[22] and PMMA[23] have been tested against QENS and neutron diffraction data and described elsewhere. For the blend simulations, we also require forces between PEO and PMMA atoms. Only nonbonded potentials, summarized in Table 1, are needed for this purpose. Integration was accomplished using a velocity−Verlet algorithm with the multiple time step reversible reference system propagator algorithm employed to reduce computation time. [41] Values for the time steps are listed in Table 2. The cutoff distance for both van der Waals and Coulomb interactions was 7 Å, with long-range electrostatic interactions calculated using the Ewald summation method.

Initial configurations were obtained from well equilibrated united atom simulations. To obtain the initial EA box from the

Table 2. Time Steps Used in the Reversible Multiple Time Step Reversible Reference System Propagator Algorithm

interaction type	time step (fs)
bonding, bending and torsion	1
van der Waals and the real part of the Coulomb Ewald summation	2
reciprocal part of the Coulomb Ewald summation	4

equilibrated united atom configuration, we must place two hydrogen atoms on the PMMA C_4 and the PEO C_2, and three hydrogen atoms on the PMMA methyls C_2 and C_3 and PEO end C_3. The two hydrogen atoms are placed on the backbone PMMA C_4 and PEO C_2 simultaneously, with the C_1-C_4-H bond angle fixed at 110°, and the C_4-H bond length fixed at 1.09 Å. Hydrogen atoms are placed on PMMA C_2 and C_3 methyl groups and PEO end C_3 in a two step process, described using PMMA C_2 as an example. The first hydrogen is placed with a fixed $O_1-C_2-H_2$ bond angle of 110°, a fixed C_2-H_2 bond length of 1.09 Å, and an $H_2-C_2-O_1-C$ torsional angle chosen at random. The remaining two hydrogen atoms are then inserted with $H_2-C_2-H_2$ angles of 110° and C_2-H_2 bond lengths of 1.09 Å. Following placement of the missing hydrogen atoms, the systems were equilibrated for at least 3 ns before collecting data over 2 ns trajectories.

Evaluation of Simulation Accuracy. We evaluate the ability of our simulations to represent the influence of mixing by examining three quantities as a function of blend composition: the scattered intensity $I(q)$ is compared with neutron diffraction, the intermediate scattering function $I(q,t)$ of PEO hydrogens is compared to QENS measurements on a hPEO/dPMMA blend, and the self-intermediate scattering function of PMMA hydrogens is compared to QENS measurements on a dPEO/hPMMA blend.

In neutron diffraction, the scattered intensity $I(q,0)$ arises from coherent scattering between pairs of atomic species i and j,[42] and does not contain information about time dependence:

$$I^{\mathrm{coh}}(q,0) = \sum_i \sum_j c_i c_j b_i^{\mathrm{coh}} b_j^{\mathrm{coh}} \frac{\sin q|r_j(0) - r_i(0)|}{q|r_j(0) - r_i(0)|} \qquad (1)$$

The positions r_i and r_j are evaluated at the same time frame, the coherent scattering length b_i^{coh} describes the interaction between neutron and nucleus, the momentum transfer $q \sim 2\pi/r$ defines the spatial scale, and c_i is the atomic species concentration. This function represents atomic packing over length scales ranging from intramolecular distances to nearest neighbor packing.

We compare the composition dependence of our simulations with that of neutron diffraction data in Figure 2. The comparison cannot be made directly because the experimental data are at 300 K, well below the T_g of PMMA where simulated systems cannot be equilibrated. Instead we examine trends with composition at 500 K for the simulated systems, and at 300 K for neutron diffraction experiments, measured at the ILL, Grenoble, France, and described in reference 33. Deuterated samples were used for all measurements. The first peak, centered near 0.9 $Å^{-1}$, is associated with intermolecular packing of PMMA. In both simulation and experiment, as more PEO is added, this peak decreases, and its position shifts slightly to smaller spatial scales. The second peak is centered near the intermolecular peak in pure PEO [$q = 1.4$ $Å^{-1}$]. Its behavior with composition differs slightly between simulated and experimental investigations. In the simulations, the peak is absent in pure PMMA and its height increases steadily with the addition of PEO, as expected. The peak position in the 10% blend is at smaller spatial scales than in the 20% and 30% blends. The experimental data follows the same trends: peak height increases with additional PEO content,

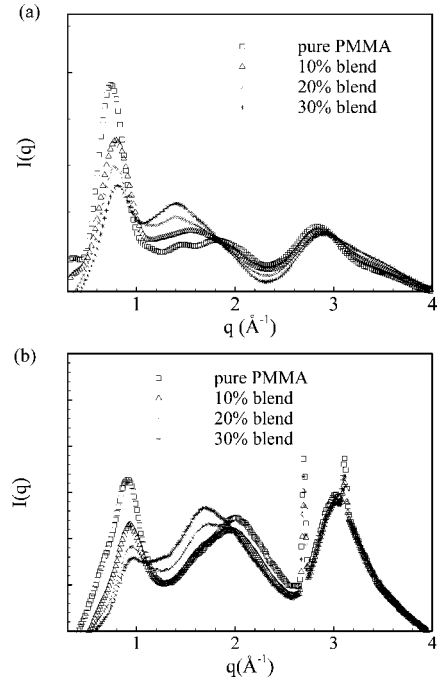

Figure 2. Static structure factors of PMMA and of PEO/PMMA blends from (a) simulations at 500 K and (b) neutron diffration experiments at 300 K.[33]

and the peak in the 10% blend is located at smaller spatial scales. The difference is in the pure PMMA curve, which has a pronounced peak at ~2 $Å^{-1}$ that is absent in the simulated data. As discussed when evaluating the simulation force field for pure PMMA, this is most likely due to differences in tacticity: the experimental samples are ~80% syndiotactic while the simulated samples are 65% syndiotactic. The features at high q are intramolecular in origin and do not change much with composition in either case. We conclude that although quantitative agreement is absent between the 300 K experimental and 500 K simulated curves, and the region surrounding the second peak has considerable disagreement, the simulation model is able to describe changes that occur with composition in a reasonable way.

The ability of the simulations to model dynamics is tested by comparison to quasi-elastic neutron scattering [QENS] data. The scattering in QENS experiments is measured in the frequency domain. Measurements performed on the High Flux Backscattering Spectrometer [HFBS][43] and the Disk Chopper Spectrometer [DCS][44] at the Center for Neutron Research, National Institute for Standards and Technology, have been described in previous publications.[32,35,37] Data obtained on these instruments are Fourier transformed to the time domain, where we compare to the intermediate scattering function calculated from simulation coordinates:

$$I(q,t) = \frac{I^{\mathrm{coh}}(q,t) + I^{\mathrm{inc}}(q,t)}{I^{\mathrm{coh}}(q,0) + I^{\mathrm{inc}}(q,0)} \qquad (2)$$

This function includes coherent and incoherent contributions, the relative weights of which are proportional to the coherent and incoherent scattering lengths [b_i^{coh} and b_i^{inc}] of the atoms present in the sample,

$$I^{\mathrm{coh}}(q,t) = \sum_i \sum_j c_i c_j b_i^{\mathrm{coh}} b_j^{\mathrm{coh}} \frac{\sin q|r_j(t) - r_i(0)|}{q|r_j(t) - r_i(0)|} \qquad (3)$$

$$I^{\mathrm{inc}}(q,t) = \sum_i c_i b_i^{\mathrm{inc}} \frac{\sin q|r_i(t) - r_i(0)|}{q|r_i(t) - r_i(0)|} \quad (4)$$

where $\vec{r}_i(t)$ is the distance vector of atom i at time t. The scattering function is normalized by the intensities at $t = 0$; the coherent part was given above, and the incoherent part is simply as follows:

$$I^{\mathrm{inc}}(q,0) = \sum_i c_i b_i^{\mathrm{inc}} \quad (5)$$

The incoherent scattering length of hydrogen is very large, and thus under most circumstances where protons are present in the samples, the scattering function is dominated by the incoherent part and can be represented with little error as

$$I^{\mathrm{self}}(q,t) = \frac{1}{\sum_i c_i b_i^{\mathrm{inc}}} \left\langle \sum_i c_i b_i^{\mathrm{inc}} \frac{\sin q|r_i(t+t_0) - r_i(t_0)|}{q|r_i(t+t_0) - r_i(t_0)|} \right\rangle = \frac{1}{N} \left\langle \sum_{i=1}^{N} \cos(q|x_i(t+t_0) - x_i(t_0)|) \right\rangle \quad (6)$$

where i indicates hydrogen atoms, and $x_i(t)$ is the x coordinate of $\vec{r}_i(t)$. The brackets indicate averages over multiple reference times, represented by t_0, rather than the single reference time of $t = 0$. We refer to this as the self-intermediate scattering function, because the incoherent part of the scattering reflects correlations between the locations of the same atoms at different times.

Experimental isolation of the mobility of one component is accomplished by "hiding" the other component with deuterium labeling: the dPEO/hPMMA system provides the motion of PMMA protons, and the hPEO/dPMMA system provides the motion of PEO protons. Because the blends that we consider are rich in PMMA, the coherent contribution from dPMMA in the hPEO/dPMMA system ranges from 25−50% of the total scattering. When comparing to data from hPEO/dPMMA blends meant to isolate the PEO component, we thus include all atoms, weighted by their coherent and incoherent cross sections, as in eqs 2, 3, and 4. When comparing with data from dPEO/hPMMA blends, we neglect the coherent contribution from dPEO, which is less than 5% of the total scattering, and calculate the motion of PMMA hydrogen atoms using eq 6. Because the mobility of the two components is well separated in time, the measurements were performed on instruments with different time ranges: PEO motion was assessed using the DCS, which covers times up to 50 ps; by this time significant decay is observed in the self-intermediate scattering function. For PMMA, we use measurements from the HFBS, covering the time range of 200 ps − 4 ns.

In Figure 3, we compare $I^{\mathrm{PMMA}}(q,t)$ obtained from the HFBS on dPEO/hPMMA blends with that calculated from the simulation, as a function of composition. We conclude that the simulations provide a good description of the influence of blending on PMMA. We note that because we present results for blends with compositions in a narrow range where crystallization is absent experimentally, the composition dependence is smaller that might otherwise be expected, in both simulation and experiment.

The intermediate scattering function $I^{\mathrm{PEO}}(q,t)$ calculated from the simulations is compared with DCS measurements on hPEO/dPMMA blends in Figure 4. Pure PEO is not included because it was only measured at 343 K. Because we did not measure the ratio of incoherent to coherent scattering in our samples, we need to include this as a variable in the comparison of simulated and experimental curves. In order to do so, we left

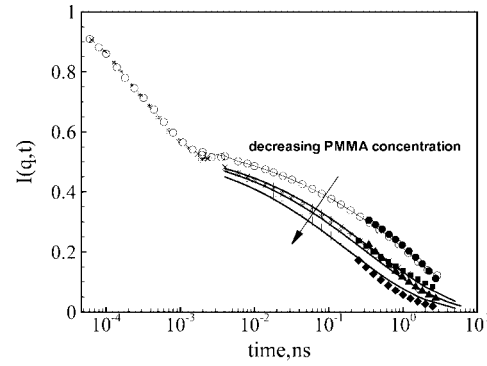

Figure 3. Comparison of simulated [open symbols] and experimental [closed symbols] self-intermediate scattering function for pure PMMA and PMMA component in the 10%, 20%, and 30% blends. Experimental data is from the HFBS on hPMMA/dPEO samples at 440 K and $q = 1.5$ Å^{-1}.[34] Simulations include the motion of all hydrogen atoms on the PMMA component at the same conditions.

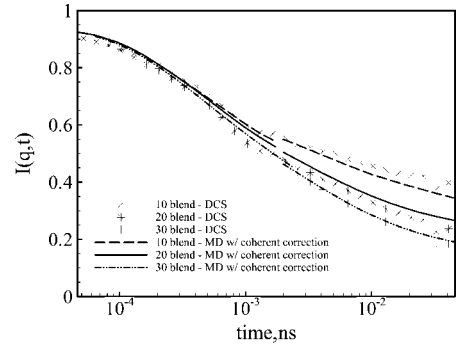

Figure 4. Comparison of simulated [lines] and experimental [symbols] self-intermediate scattering function for the PEO component in the 10%, 20%, and 30% blends. Experimental data is from the DCS on dPMMA/hPEO samples at 440 K and $q = 1.1$ Å^{-1}.[37] Simulations include both incoherent scattering from the PEO component and coherent scattering from the PMMA component.

the incoherent cross sections at their theoretical values, and multiplied the coherent cross sections by a constant value. In order to produce the agreement in Figure 4, the coherent cross sections were multiplied by 0.79 [10% blend], 0.83 [20% blend] and 0.86 [30% blend]. This is consistent with reference 36, in which the measured ratio of coherent to incoherent scattering at $q = 1.1$ Å^{-1} is 90% of that anticipated by the theoretical cross sections for a 25% PEO/75% PMMA blend. At first glance, it appears that the influence of mixing is greater on PEO than on PMMA. As mentioned above, the experimental data contains a contribution from dPMMA, which is immobile on the time scale of the instrument; its contribution to the measurement is to increase the value to which the function will decay from zero to some fraction consistent with the amount of PMMA in each blend. An examination of this issue in conjunction with experimental measurements is presented in ref 37, where it is concluded that the contribution from dPMMA is elastic up to 470 K, as can be seen from the tendency of the data to level off toward the end of the time range. Although we include this contribution for comparison to experimental data, it was removed from our experimental study by including an elastic fraction in the fitting procedure, and it is removed in the current study by excluding PMMA atoms from the calculation. As will be seen below, this decreases the influence of mixing. Although the PEO component requires an additional adjustable parameter [the ratio of coherent to incoherent scattering], its value is consistent with available experimental measurements. We thus conclude that the simulation model is able to adequately capture changes in PEO dynamics that occur with mixing,

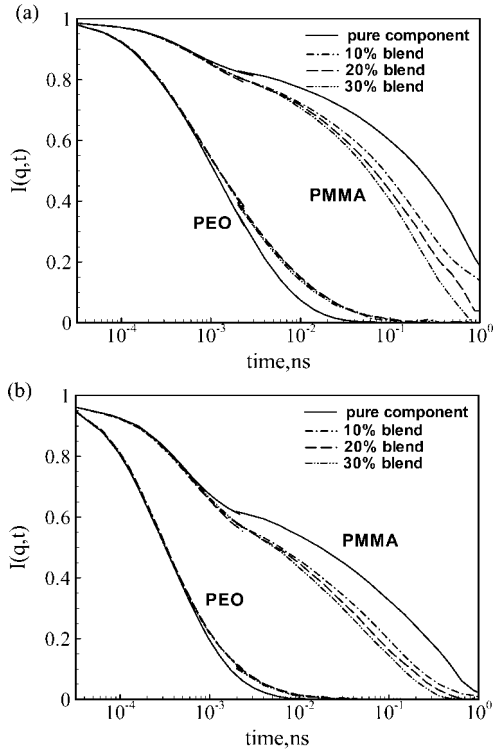

Figure 5. Influence of mixing on the segmental relaxations of PEO and PMMA at 500 K and (a) $q = 0.9$ Å^{-1}; (b) $q = 1.5$ Å^{-1}. For PEO, we include all hydrogen atoms, whereas for PMMA we include only those on the chain backbone to isolate the segmental relaxation.

although this observation is not as strong as for the PMMA component.

The Effect of Environment on the Primary Relaxations of PEO and PMMA. We begin by comparing the influence of mixing on the primary relaxations of the two components. To do so, we consider the self-intermediate scattering function of hydrogen atoms, as with QENS experiments. The primary relaxation is isolated in PMMA by considering motion of only the backbone hydrogen atoms, eliminating methyl group rotations and the β-relaxation.[24] For PEO, we consider all the hydrogen atoms. These data may be regarded as a "perfect" QENS experiment: one with exact labeling and ability to remove the secondary relaxations in PMMA. The two functions are compared in Figure 5. Decays for both components consist of two processes: a composition-independent decay before 1 ps, followed by a second decay that is influenced by environment. The fast decay is a common feature in polymers, observed for PEO,[37,45] PMMA,[24,35] and other polymers.[46−48] Physically, it represents atomic motion prior to encountering constraints formed by other atoms, and has been connected with oscillations within a torsional well.[49] The time 1 ps is also the time where the mean-squared displacement crosses from the ballistic to subdiffusive regimes, illustrated in Figure 6. We use ballistic to refer to the initial motion before encountering other atoms, rather than the mean-squared displacement going as t,^{2} which is sometimes associated with this term. For polymer melts, the mean squared displacement in the ballistic region is often between t^1 and $t^{1.5}$. The time of cross-over appears material independent, but the distance the atoms have traveled at that time [the local cage size] is quite different. Specifically, the cage for PEO is almost twice as large as that of PMMA: as defined by $(\mathrm{MSD})^{1/2}$, the cage radii are 2.2 Å for PEO and 1.2 Å for PMMA. This is reflected in the decay curves. The spatial scale $q = 1.5$ Å^{-1} corresponds roughly to motion within a sphere of radius 2.1 Å, approximately equal to the cage size for PEO.

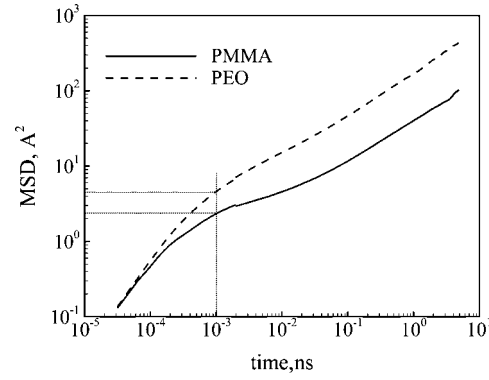

Figure 6. Mean-squared displacements [MSD] of both components in the 20% blend at 500 K.

We thus expect a significant portion of the PEO decay will reflect cage exploration. The observation that the fast decay occupies about 80% of the total decay is consistent with this expectation. This is relevant for PEO because the cage size is unusually large, and motion of the second, composition dependent process is unusually fast. This combination means that at spatial scales where the second process would normally be visible, the decay curve reflects mainly fast cage exploration instead. If this cage exploration is connected with torsional oscillations, as was shown for poly(ethylene),[49] they are unusually large, and likely enable fast barrier crossings. We explore this possibility in Figure 7, in which the behavior of the backbone dihedral angles is illustrated as a function of time. Rotation about the C−C bond occurs by brief residences with oscillations about torsional minima, interspersed with regions of time where rotation appears to occur freely. Only this behavior is observed for rotation about the C−O bond. This means that the typical time required for rotation about this bond is less than 2 ps. In PEO, the decay on the time scale normally connected with torsional oscillations also includes significant torsional barrier crossings. This greatly increases the average area explored by the PEO protons and leads to the unusually strong fast decay in PEO. Blending with PMMA has little influence on this conclusion.

The second process, beginning at ∼1 ps, is associated with the primary relaxations of each component. This behavior of this process is consistent with previous observations: the primary relaxation of PMMA is significantly influenced by environment, while that of PEO is not.[30−37] In particular, the observation that PEO mobility is slowed slightly when mixed with PMMA, with the extent independent of composition is consistent with deuterium NMR experiments on this system.[31]

To summarize the decays for the entire temperature and spatial scale range of our simulations, we extract a characteristic time from $I^{\mathrm{PEO}}(q,t)$ or $I^{\mathrm{PMMA}}(q,t)$ using the empirical Kolrausch−Williams−Watts [KWW] expression:

$$I(q,t) = A \exp\left[-\left(\frac{t}{\tau_{\mathrm{KWW}}}\right)^{\beta}\right] \tag{7}$$

While the KWW expression is empirical, the three parameters have physical significance: A represents the strength of processes faster than the time window of fitted data, τ_{KWW} is the characteristic time of the observed motion, and β indicates the width of the characteristic time distribution.

The characteristic times of both components are presented as a function of temperature for all blend compositions in Figure 8. Experimental data is provided for comparison: for PMMA, we choose a momentum transfer of $q = 0.6$ Å^{-1} and compare to QENS data: at this momentum transfer the primary relaxation contributes most to the observed scattering.[32] For PEO, experi-

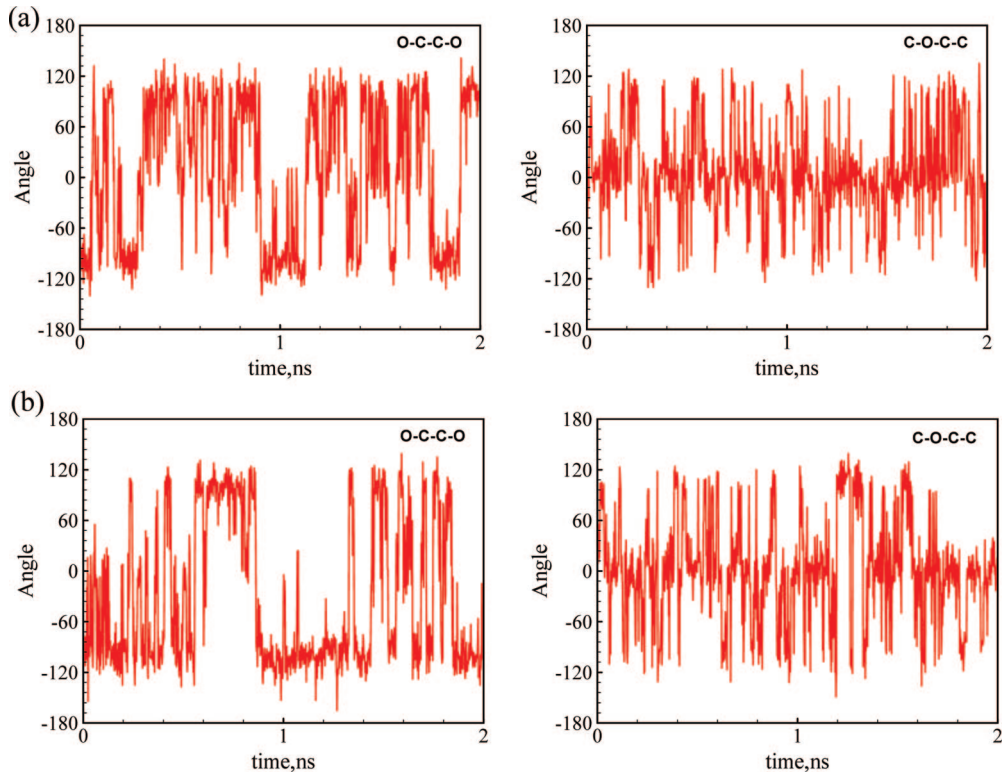

Figure 7. Dihedral angles as a function of time with the time interval of 2 ps at 400 K for (a) pure PEO and (b) PEO in 20% blend.

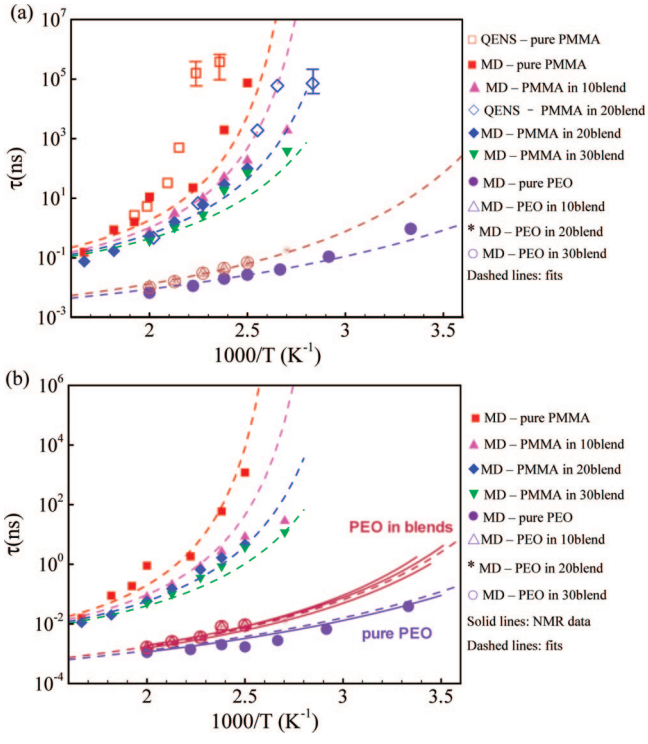

Figure 8. Temperature dependence of segmental relaxation times of PMMA and PEO in all three blends at (a) $q = 0.6$ Å^{-1} and (b) $q = 1.5$ Å^{-1}. QENS[32] and NMR[31] data are also included in this figure for comparison.

mental data other than our own is available. We thus include relaxation times from NMR[13] and choose a momentum transfer of $q = 1.5$ Å^{-1}: this provides the best comparison between neutron and NMR data, indicating that the length scale for reorientation of a C−H bond is approximately 4 Å. The error bars provided with the QENS data indicate the range of relaxation times that can describe the measured decay, regardless of the values of other fit parameters, as discussed in reference 32. As shown in Figure 8a, times for the PMMA primary relaxation isolated using simulation correspond to the QENS data, both with respect to their values and the influence of the faster PEO. When the absolute values of relaxation times are large, such as the lowest temperatures for pure PMMA, quantitative agreement is lost. This is not surprising, as the error bars for the experimental points increase and the simulation is least reliable under these conditions. The same is true for the PEO primary relaxation: as illustrated in Figure 8b, the times correspond well to those measured via NMR. Characteristic times for PMMA change significantly with addition of PEO, but only moderately as the amount of PEO increases. We present the stretching parameters for both components in Figure 9. Stretching parameters for the primary relaxation of PMMA are highly temperature dependent, as also observed by dielectric spectroscopy, presented for comparison. Blending does not change the stretching parameters for PMMA, indicating that the breadth of the relaxation time distribution is insensitive to blending. The situation is different for PEO, where blending with PMMA significantly decreases the stretching parameter, consistent with a wider distribution of relaxation times. The temperature dependence is similar to that reported by Genix, et al.[36] for a 10 wt % PEO blend, also shown for comparison. The wider distribution could have several causes: confinement effects at temperatures below the blend T_g, and two populations of PEO protons differing in their response to blending with PMMA are both consistent with a wider distribution. Small values of the stretching parameter that depend on temperature [around 0.3 from NMR,[13] ranging from 0.35 at 307 K to 0.5 at 444 K for QENS[37]] are consistent with experimental measurements on PEO. As suggested by the decay curves, times characterizing the primary relaxation for PEO are insensitive to composition: times from the three blends, although displaced slightly from pure PEO, are coincident. As mentioned in the

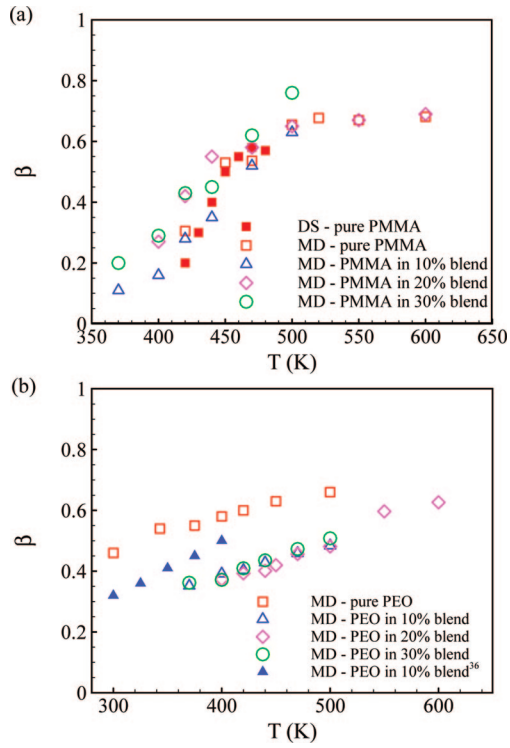

Figure 9. Temperature dependence of β for the segmental relaxations of both components. Both graphs are for $q = 0.6$ Å^{-1}: (a) PMMA compared to dielectric spectroscopy;[50] (b) PEO compared to MD data from ref 36.

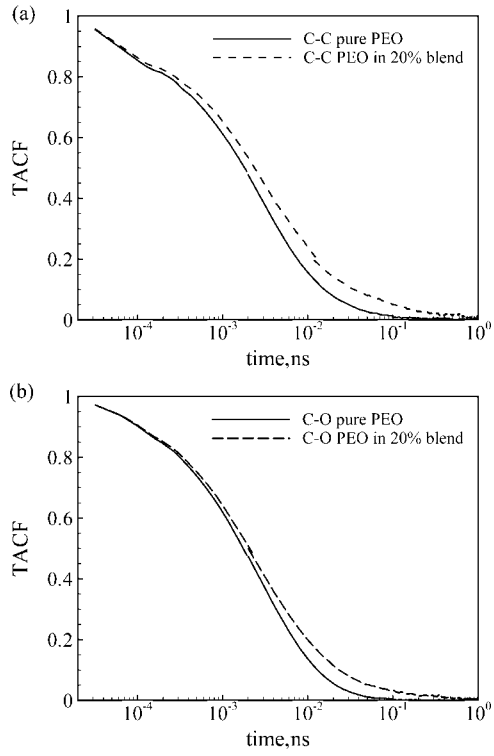

Figure 10. Torsional autocorrelation function for pure PEO and PEO in 20% blend at 400 K: (a) C−C bond; (b) C−O bond.

introduction, this unusual observation has spurred a number of explanations.

One is that the lack of side groups on the PEO chain decouples it from its environment.[31] Another is that the observed relaxation is a secondary, or β-relaxation, which is related to single transitions between torsional minima and is always present, even when merged with the primary relaxation, which is associated with exploration of torsional minima with equilibrium probability.[28] Techniques such as deuterium NMR, QENS and simulation, which probe high frequency processes, would be sensitive to the β-relaxation rather than the primary relaxation. Finally, it has been suggested that the influence of the surrounding environment is small for PEO because its primary relaxation time is small enough that it approaches the primitive relaxation (the process appearing at times less than 1 ps).[39]

Table 3. VTF Fit Parameters for PMMA and PEO Dynamics in Blends[a]

	pure PMMA	PMMA in 10% blend	PMMA in 20% blend	PMMA in 30% blend
T_g (K)	373	349	327	309
T_0 (=T_g − 33 K)	340	316	294	276
	pure PEO		PEO in all three blends	
T_0 (K)	166		212	

[a] For fits to PMMA dynamics $B = 795$ K, $\tau_\infty = 10.8$ ps for $q = 0.6$ Å^{-1}, and $\tau_\infty = 1$ ps for $q = 1.5$ Å^{-1}; for fits to PEO dynamics $B = 850$ K, $\tau_\infty = 0.1$ ps for $q = 0.6$ Å^{-1}, and $\tau_\infty = 1$ ps for $q = 1.5$ Å^{-1}.

It appears that despite having very small characteristic times, the relaxation observed is the primary relaxation. As presented in Figure 7 above, there are two distinct backbone rotations for PEO. Many of the rotations about both types of bonds occur in less than 2 ps, but some larger residence times are observed, particularly about the C−C bond. Because the typical time scale for one conformational transition is less than 1 ps, the lowest time we used when fitting the data, the observed process cannot be the β-relaxation. The process appearing in the time window we fit corresponds to the latter stage, composition dependent decay of the torsional autocorrelation function, as illustrated in Figure 10. Characteristic times obtained from fitting the data longer than 1 ps are consistent with those in Figure 8. The small environmental influence is thus a real feature of the α-relaxation in PEO. It appears that in PEO, the β-relaxation is so fast that it is merged with torsional oscillations and thus not observed, rather than the α- relaxation being so fast it is dominated by the β-relaxation. To the extent that the primitive relaxation time may be regarded as the time for exploration within a torsional well, the interpretation of reference 39 is accurate.

Also provided in Figure 8 are attempts to correlate the data with Vogel−Tamman−Fulcher (VTF) fits using pure component parameters:

$$\ln\left(\frac{\tau}{\tau_\infty}\right) = \frac{B}{T - T_0} \tag{8}$$

The composition dependence is introduced via T_0, while τ_∞ and B retain pure component values for blend fits. The resulting parameters are listed in Table 3. For PMMA, we require that T_0 follow the composition dependence of T_g, as prior QENS measurements have suggested this is appropriate. For PEO, T_0 is treated as a free parameter. Although the temperature dependence of the pure components is captured by these fits, the composition dependence for PMMA is not well described. This means that primary relaxation times for the simulated blends cannot be described by changes in blend T_g, as is possible for QENS measurements. This may be due to the shorter chains used for the simulations, for which measured T_gs may not be appropriate.

We present the spatial dependence of characteristic times in Figure 11. For PMMA at all compositions, characteristic times follow a power law in momentum transfer: $\tau_{KWW} \sim q^{-2/\beta}$, consistent with translational motion. For PEO, two scaling regions are evident, with a cross-over near $q = 1$ Å^{-1}. At spatial

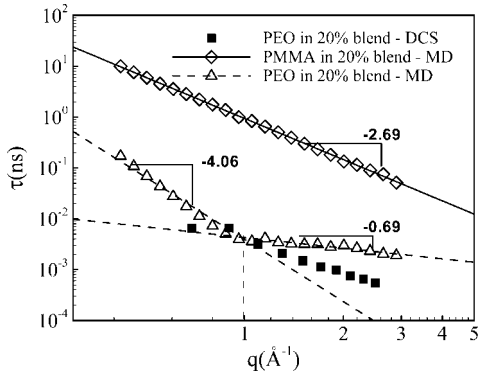

Figure 11. Dependence of segmental relaxation times on spatial scale for both components in the 20% blend at 440 K. DCS data are also included.[37]

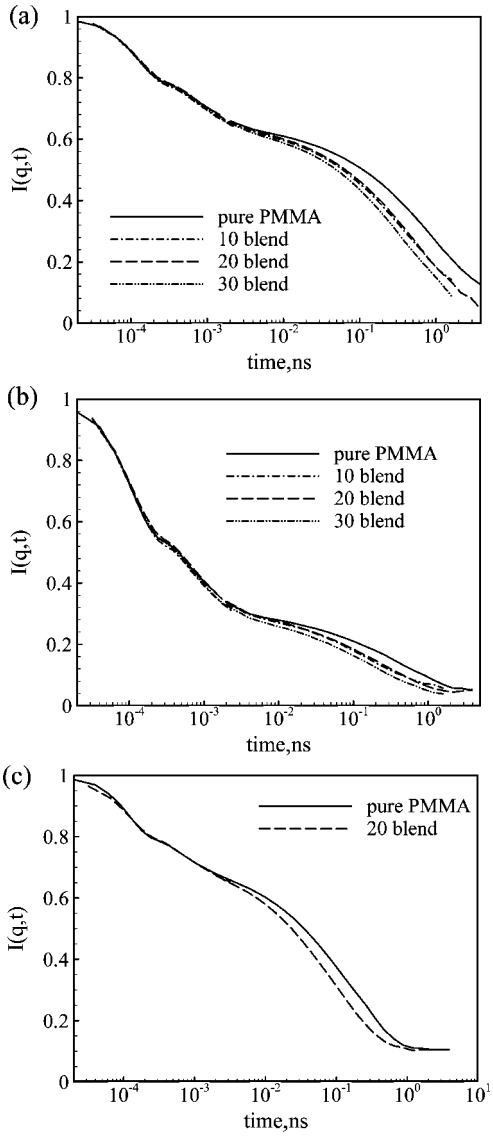

Figure 12. Influence of blending with PEO on the rotation of the entire ester group of PMMA. Data shown are (a) $q = 0.9$ Å^{-1} and $T = 500$ K; (b) $q = 0.8$ Å^{-1} and $T = 500$ K; (c) $q = 1.5$ Å^{-1} and $T = 600$ K.

scales larger than this, Rouse scaling is observed, whereas at smaller spatial scales, the characteristic times change only slightly. This type of scaling is a hallmark of restricted motion, such as rotation, and was previously reported in simulations of this system at temperatures lower than we consider here.[36] In

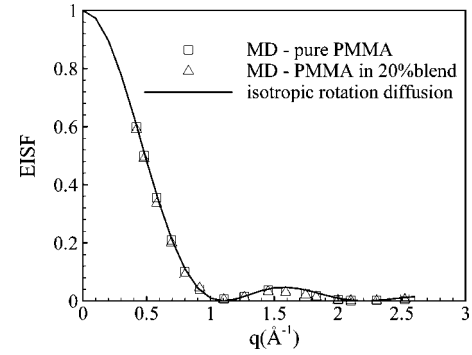

Figure 13. Spatial dependence of the EISF obtained from rotation of the entire ester side group in pure PMMA and in the 20% blend at 600 K. Data are consistent with isotropic rotational diffusion over a sphere of radius 2.85 Å.

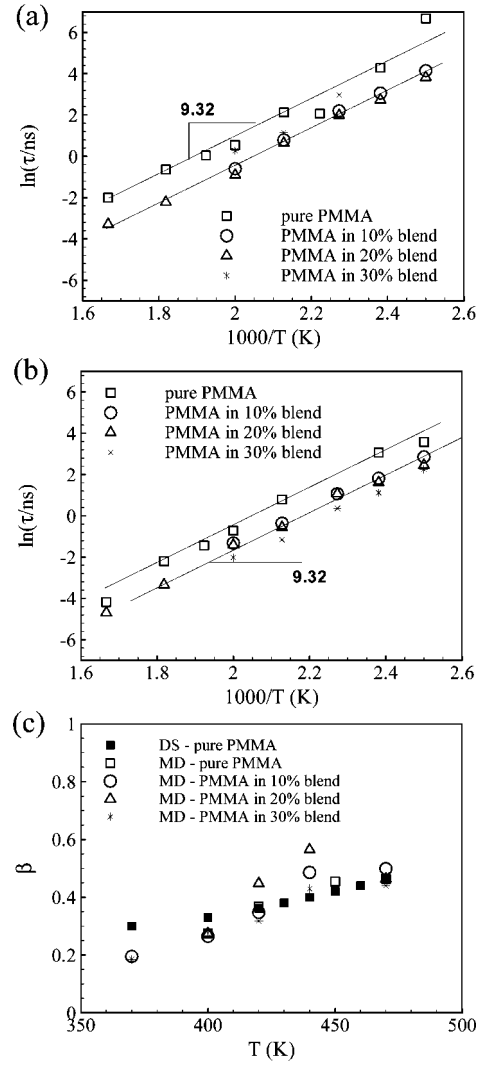

Figure 14. Temperature dependence of entire ester group rotational times and stretching parameters in pure PMMA and all blends at (a) relaxation times at $q = 0.6$ Å^{-1}, (b) relaxation times at $q = 1.5$ Å^{-1}, and (c) stretching parameters at $q = 1.5$ Å^{-1}.

that case, this behavior was attributed to restriction of PEO motion due to the immobile PMMA component, as all considered temperatures were lower than the glass transition for PMMA. That is not the case here, although such an interpretation is still possible due to the 2−3 orders of magnitude separating the characteristic times of the two components. We reported a similar change in slope from QENS data, and those

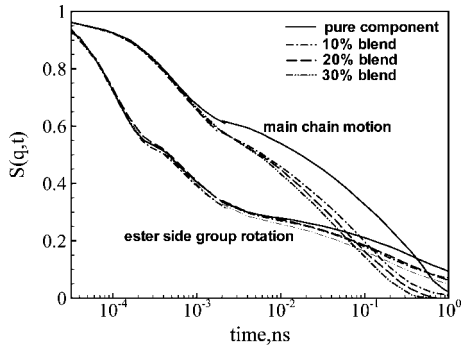

Figure 15. Comparison of the composition dependence of segmental motion of PMMA and ester group rotation at 500 K.

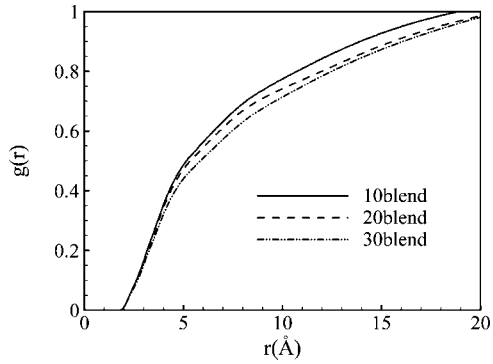

Figure 16. PEO−PMMA intermolecular pair distribution function for all blends at 500 K.

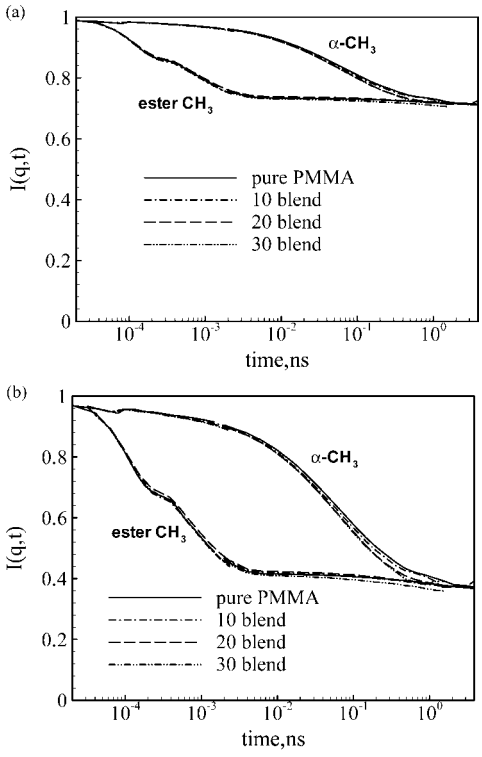

Figure 17. Comparison of methyl group rotations in pure PMMA and PEO/PMMA blends at 500 K: (a) $q = 0.9$ Å^{-1}; (b) $q = 1.5$ Å^{-1}.

times are included in Figure 11.[37] It can be difficult to distinguish Rouse [$\tau_{KWW} \sim q^{-4}$] from translational [$\tau_{KWW} \sim q^{-2/\beta}$] motion for polymers since β is frequently near 0.5]. This is also the case here, since values of β for PEO range from 0.4 to 0.5.

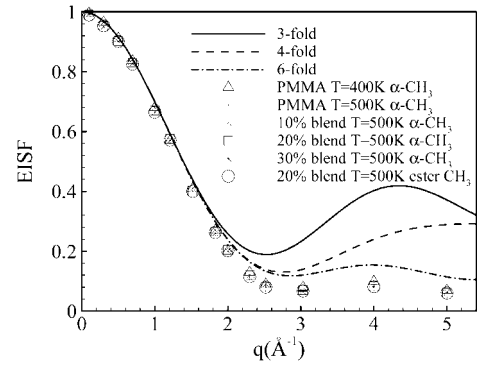

Figure 18. Spatial dependence of the EISF obtained from methyl group rotation in pure PMMA and in the blends at 500 K. Pure PMMA is also shown at 400 K. Data are most consistent with the 6-fold rotation model.

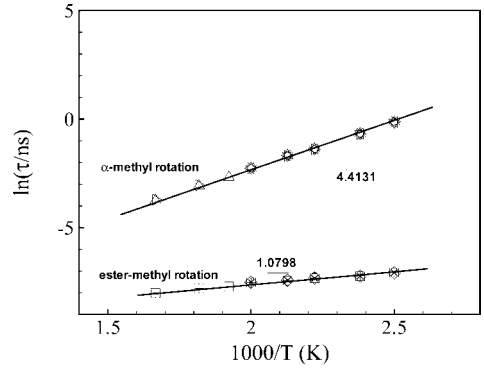

Figure 19. Temperature dependence of methyl group rotations in pure PMMA and PEO/PMMA blends at $q = 0.6$ Å^{-1}. Rotational times are q-independent.

The Effect of Environment on Secondary Relaxations in PMMA. We now turn our attention from the primary relaxation to the behavior of the three secondary relaxations in PMMA when mixed with PEO. For pure PMMA, we previously connected rotation of the ester side group with the β-relaxation by showing that it is an activated process with activation energy consistent with dielectric spectroscopy measurements of the β-relaxation at low temperature.[50] To isolate either ester or methyl group rotations, we calculate $I(q,t)$ using eq 6, but neglecting translational motion by "virtually fixing" the terminal position of the rotating group. For example, to isolate ester methyl group rotation, we fix the C_2 position [see Figure 1], whereas to isolate rotation of the ester side group, we fix the C position. Clearly, these carbon atoms do move throughout the simulation: their position is rendered fixed by calculating the hydrogen positions relative to the position of the appropriate carbon atom.

The intermediate scattering function describing ester group rotation $I^{ester}(q,t)$ is presented in Figure 12. In contrast to the behavior of the β-relaxation at low temperature, at temperatures where the main chain relaxes over comparable times, the β-relaxation is influenced by addition of PEO. The nature of the influence is reminiscent of the primary relaxation in PEO: the decay is faster when PEO is present, but the extent of the difference is composition independent. Because data for the three blends are nearly coincident, in what follows, we examine the behavior of the 20% blend in comparison to pure PMMA. To fit the decays and obtain characteristic times, we use a variant of the KWW expression relevant for rotational motion:

$$I(q,t) = A\left\{\mathrm{EISF} + (1 - \mathrm{EISF})\exp\left[-\left(\frac{t}{\tau_{KWW}}\right)^{\beta}\right]\right\} \quad (9)$$

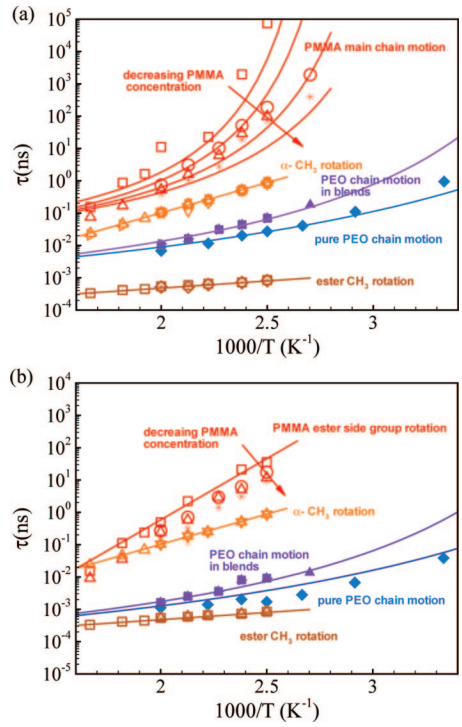

Figure 20. Relaxtion time map for the PEO/PMMA blends. Both parts [color online]: orange, α-methyl rotation; purple, primary relaxation of PEO in blends; blue, primary relaxation of pure PEO; brown ester methyl rotation. Part a is for $q = 0.6$ Å^{-1} and shows PMMA primary relaxations in red. Part b is for $q = 1.5$ Å^{-1} and shows PMMA ester side group rotation in red. Solid symbols indicate pure component data.

This approach[51,52] allows for a distribution of rotational times, and yields fit qualities comparable to a log-Gaussian distribution, frequently used to describe rotation of side groups. The parameters A, τ_{KWW}, and β retain the same meanings, and the EISF [elastic incoherent structure factor] describes motion over a restricted spatial area, with the q dependence of the EISF characterizing its geometry. A plateau in $I(q,t)$ at long times indicates the presence of an EISF and sets its value. Clear assignment of the value of the EISF requires running until the plateau is well established, something that is less computationally demanding at high temperatures. The EISF for rotation is temperature independent, and thus we choose 600 K to set its value and use this to fit the data at other temperatures. The EISF in pure PMMA and in the 20% blend are coincident, as illustrated in Figure 13, from which we determine that the EISF is composition independent. Although they are not used for illustration purposes, fits to the other two blend compositions were made using this same EISF.

The information in Figure 13 can be used to determine the geometry and type of rotation. Because the rotating protons are separated from the point of rotation by three bonds, we expect rotation of the ester group to occur in a continuous manner. We thus provide the prediction of the isotropic rotational diffusion model, in which continuous small angle rotations occur and the rotating molecule has no preferred spatial orientation:

$$\mathrm{EISF} = \left(\frac{\sin(qr)}{qr}\right)^2 \tag{10}$$

In the above equation, $r = 2.85$ Å represents the radius of the area of rotation. As shown in Figure 13, this model provides an excellent description of the EISF for both pure PMMA and the 20% blend. This suggests that ester methyl protons rotate around the C_1-C bond by randomly moving throughout a circle of radius 2.85 Å. The rotation of the ester group in PMMA has previously been investigated using simulation.[53] The authors used a different approach to isolate the rotation, by fitting the decay of ester group hydrogens with a function that describes both segmental motion and rotation. As in the current case, these authors find that the extent of the rotation is large [~4 Å], but conclude that rotation on a circle [8 or more sites] is more appropriate.

We compared the temperature dependence of ester group rotation in pure PMMA to experimental measurements of the β-relaxation in a previous publication,[24] and concluded that our simulation results are consistent with the high temperature end of the β-relaxation. As with pure PMMA, the temperature dependence of characteristic times for ester group rotation in the blends [Figure 14a] is Arrhenius. The activation energy is consistent with dielectric measurements as previously discussed.[24] Although the barrier remains constant, the presence of PEO shortens the relaxation times. As mentioned above, this is different than the usual observation at low temperature; that the β-relaxation is uninfluenced by environment. The stretching parameters for ester group rotation vary with temperature, as illustrated in Figure 14c. The temperature dependence is slightly larger than that obtained for dielectric measurements, but within the scatter of the data. We note that dielectric spectroscopy only observes the β-relaxation and the primary relaxation of PMMA as distinct processes below the T_g of PMMA: above this temperature they appear to merge into a single process. The current measurements isolate the motion responsible for the β-relaxation[24,54] at high temperature. It appears that in this region, relaxation times for the primary relaxation and the β-relaxation of PMMA are both influenced by mixing. This is evident from Figure 15, in which the composition dependence of both processes is presented in a single graph. The decays of main chain motion and ester group rotation occur over similar time scales, consistent with their merging to a single process in this temperature range in dielectric experiments. The main chain motion is clearly influenced more by the presence of the fast PEO than ester group rotation, and a stronger composition dependence is also evident. Given that the ester group rotates over an area approximately 6 Å in diameter, and that significant packing of PEO with PMMA occurs over this spatial range as illustrated by the PEO−PMMA intermolecular $g(r)$ in Figure 16, it is reasonable that PEO atoms are encountered as this group rotates, thus influencing its mobility.

PMMA has two methyl groups, one located on the ester side chain [C_2] and the other attached to the main chain branch point [C_3], termed the α-methyl. The ester methyl rotates quickly [times in the ps range at the temperatures of our simulations], while α-methyl rotation times are comparable to those of the primary and β-relaxations. We calculate the intermediate scattering function reflecting rotation of both methyl groups as described above. The results, presented in Figure 17, show that methyl group rotation in PMMA is insensitive to environment. A slight influence on the α-methyl can be discerned at high q, but this is much smaller than the influence on ester side group rotation. To obtain characteristic times and describe the entire temperature range, we fit the data using eq 9, with the EISF assigned from the plateau values in $I^{methyl}(q,t)$. The EISF is temperature and composition independent, the same for both methyl groups, and most consistent with a 6-fold rotation model,[55] as illustrated in Figure 18. The 6-fold model describes motion between six equally spaced sites on a sphere, and captures the combination of motion within a site combined with site transitions better than a 3-fold model. This is an unexpected result that we attribute to the high temperature of the simulation compared to where methyl group rotation is normally measured. A full discussion can be found in reference 55. Methyl group

relaxation times are presented as a function of temperature in Figure 19. As expected, the coincidence of methyl group rotation for pure PMMA and PMMA in blends with PEO is observed over the entire temperature range: both relaxation times themselves, and activation energies are insensitive to environment. One might ask why rotation of the entire ester group is sensitive to environment, whereas rotation of the methyl group itself is not. The spatial extent of the two motions is quite different: the ester group rotates over a sphere of radius 2.85 Å, whereas the methyl group rotates over a hexagon that can be inscribed in a sphere of radius 1.02 Å. In the former case, the protons travel over distances comparable to interchain spacings, and thus as discussed above have the opportunity for their motion to be influenced by the surrounding PEO chains. Since the closest intermolecular contacts occur at 2.7 Å, it is not possible for interchain packing to influence rotation of the smaller methyl groups.

Concluding Remarks

We summarize with a relaxation map in Figure 20, which illustrates the responses of the five motions investigated in the paper to mixing: the primary relaxations of PEO and PMMA, the β-relaxation in PMMA, and rotation of the two PMMA methyl groups. Both parts of the figure present the primary relaxations of PEO, and rotational times for the PMMA methyls. In part a, we show the primary relaxation of PMMA, whereas in part b the β-relaxation of PMMA is presented. The different relaxations overlap significantly, in particular the primary and β-relaxations in PMMA, and to some extent rotation of the α-methyl. At the higher momentum transfer, $q = 1.5$ Å^{-1}, times for PEO approach rotation of the ester methyl in PMMA. The β-relaxation in PMMA becomes faster when the environment is altered to include PEO. It thus appears that localized motions may be influenced by environment if the spatial extent of the motion is sufficiently large.

Acknowledgment. Financial support from the National Science Foundation, Polymers Program, Grant DMR-0134910 is gratefully acknowledged. This work utilized facilities supported in part by the National Science Foundation under Agreement No. DMR-0454672.

References and Notes

(1) Gómez, D.; Alegría, A.; Arbe, A.; Colmenero, J. *Macromolecules* **2001**, *34*, 503–513.
(2) Arbe, A.; Ritchter, D.; Colmenero, J.; Farago, B. *Phys. Rev. E* **1996**, *54*, 3853–3869.
(3) Bieze, T. W. N.; van der maarel, J. R. C.; Eisenbach, C. D.; Leyte, J. C. *Macromolecules* **1994**, *27*, 1355–1366.
(4) Zhu, W.; Gisser, D. J.; Ediger, M. D. *J. Polym. Sci., Polym. Phys.* **1994**, *32*, 2251–2262.
(5) Merenga, A. S.; Papadakis, C. M.; Kremer, F.; Liu, J.; Yee, A. F. *Colloid Polym. Sci.* **2001**, *279*, 1064–1072.
(6) Arbe, A.; Monkenbusch, M.; Stellbrink, J.; Richter, D.; Farago, B.; Almdal, K.; Faust, R. *Macromolecules* **2001**, *34*, 1281–1290.
(7) Ding, Y.; Sokolov, A. P. *Macromolecules* **2006**, *39*, 3322–3326.
(8) Cendoya, I.; Alegria, A.; Alberdi, J. M.; Colmenero, J.; Grimm, H.; Richter, D.; Frick, B. *Macromolecules* **1999**, *32*, 4065–4078.
(9) Hoffmann, S.; Willner, L.; Ritchter, D.; Arbe, A.; Colmenero, J.; Farago, B. *Phys. Rev. Lett.* **2000**, *85*, 772–775.
(10) Doxastakis, M.; Kitsiou, M.; Fytas, G.; Theodorou, D. N.; Hadjichristidis, N.; Meier, G.; Frick, B. *J. Chem. Phys.* **2000**, *112*, 8687–8694.
(11) Chung, G. C.; Kornfield, J. A.; Smith, S. D. *Macromolecules* **1994**, *27*, 5729–5741.
(12) Leroy, E.; Alegría, A.; Colmenero, J. *Macromolecules* **2003**, *36*, 7280–7288.
(13) He, Y.; Lutz, T. R.; Ediger, M. D. *J. Chem. Phys.* **2003**, *119*, 9956–9965.
(14) Lodge, T. P.; McLeish, T. C. B. *Macromolecules* **2000**, *33*, 5278–5284 .
(15) Kumar, S. K.; Colby, R. H.; Anastiasadis, S. H.; Fytas, G. *J. Chem. Phys.* **1996**, *105*, 3777–3786.
(16) Roland, C. M.; Ngai, K. L. *Macromolecules* **1991**, *24*, 2261–2265.
(17) Zawada, J. A.; Ylitalo, C. M.; Fuller, G. G.; Colby, R. H.; Long, T. E. *Macromolecules* **1992**, *25*, 2896–2902.
(18) Zetsche, A.; Fischer, E. W. *Acta Polym.* **1994**, *45*, 168–175.
(19) Katana, G.; Fischer, E. W.; Hack, T. H.; Abetz, V.; Kremer, F. *Macromolecules* **1995**, *28*, 2714–2722.
(20) Mukhopadhyay, R.; Alegría, A.; Colmenero, J.; Frick, B. *J. Non-Cryst. Solids* **1998**, *235*−*237*, 233–236.
(21) Arrighi, V.; Higgins, J. S.; Burgess, A. N.; Howells, W. S. *Macromolecules* **1995**, *28*, 4622–4630.
(22) Chen, C. X.; Depa, P.; García Sakai, V.; Maranas, J. K.; Lynn, J. W.; Peral, I.; Copley, J. R. D. *J. Chem. Phys.* **2006**, *124*, 234901/1–11.
(23) Chen, C. X.; Depa, P.; Maranas, J. K.; García Sakai, V. *J. Chem. Phys.* **2008**, *128*, 124906/1–10.
(24) Chen, C. X.; Maranas, J. K.; García Sakai, V. *Macromolecules* **2006**, *39*, 9630–9640.
(25) Jin, X.; Zhang, S.; Runt, J. *Polymer* **2002**, *43*, 6247–6254.
(26) Elmahdy, M. M.; Chrissopoulou, K.; Afratis, A.; Floudas, G.; Anastasiadis, S. *Macromolecules* **2006**, *39*, 5170–5173.
(27) Smith, G. D.; Bedrov, D. *J. Non-Cryst. Solids* **2006**, *352*, 4690–4695.
(28) Bedrov, D.; Smith, G. D. *Macromolecules* **2006**, *39*, 8526–8535.
(29) Ito, H.; Russell, T. P.; Wignall, G. D. *Macromolecules* **1987**, *20*, 2213–2220.
(30) Dionísio, M.; Fernandes, A. C.; Mano, J. F.; Correia, N. T.; Sousa, R. C. *Macromolecules* **2000**, *33*, 1002–1011.
(31) Lutz, T. R.; He, Y.; Ediger, M. D.; Cao, H.; Lin, G.; Jones, A. A. *Macromolecules* **2003**, *36*, 1724–1730.
(32) García Sakai, V.; Chen, C. X.; Maranas, J. K.; Chowdhuri, Z. *Macromolecules* **2004**, *37*, 9975–9983.
(33) Farago, B.; Chen, C. X.; Maranas, J. K.; Kamath, S.; Colby, R. H.; Pasquale, A. J.; Long, T. E. *Phys. Rev. E* **2005**, *72*, 031809/1–11.
(34) Liu, J.; García Sakai, V.; Maranas, J. K. *Macromolecules* **2006**, *39*, 2866–2875.
(35) García Sakai, V.; Maranas, J. K.; Chowdhuri, Z.; Peral, I.; Copley, J. R. D. *J. Polym. Sci., Part B: Polym. Phys* **2005**, *43*, 2914–2922.
(36) Genix, A.-C.; Arbe, A.; Alvarez, F.; Colmenero, J.; Willner, L.; Ritchter, D. *Phys. Rev. E* **2005**, *72*, 031808/1–20.
(37) García Sakai, V.; Maranas, J. K.; Peral, I.; Copley, J. R. D. *Macromolecules* **2008**, *41*, 3701–3708.
(38) Colby, R. H. *Polymer* **1989**, *30*, 1275–1278.
(39) Ngai, K. L.; Roland, C. M. *Macromolecules* **2004**, *37*, 2817–2822.
(40) Berendsen, H. J. C.; Postma, J. P. M.; van Gunsteren, W. F.; DiNola, A.; Haak, J. R. *J. Chem. Phys.* **1984**, *81*, 3684–3690.
(41) Tuckerman, M.; Berne, B. J.; Martyna, G. J. *J. Chem. Phys.* **1992**, *97*, 1990–2001.
(42) Borodin, O.; Douglas, R. J.; Smith, G. D.; Trouw, F.; Petrucci, S. *J. Phys. Chem. B* **2003**, *107*, 6813–6823.
(43) Meyer, A.; Dimeo, R. M.; Gehring, P. M.; Neumann, D. A. *Rev. Sci. Instrum.* **2003**, *74*, 2762–2770.
(44) Copley, R. D.; Cook, J. C. *Chem. Phys.* **2003**, *292*, 477–485.
(45) Sacristan, J.; Chen, C. X.; Maranas, J. K. *Macromolecules* **2008**, *41*, 5466–5475.
(46) Colmenero, J.; Arbe, A.; Coddens, G.; Frick, B.; Mijangos, C.; Reinecke, H. *Phys. Rev. Lett.* **1997**, *78*, 1928–1931.
(47) Zorn, R.; Arbe, A.; Colmenero, J.; Frick, B.; Richter, D.; Buchenau, U. *Phys. Rev. E* **1995**, *52*, 781–795.
(48) Buchenau, U.; Wischnewski, A.; Richter, D.; Frick, B. *Phys. Rev. Lett.* **1996**, *77*, 4035–4038.
(49) Arialdi, G.; Ryckaert, J.-P.; Theodorou, D. N. *Chem. Phys.* **2003**, *292*, 371–382.
(50) Bergman, R.; Alvarez, F.; Alegría, A.; Colmenero, J. *J. Chem. Phys.* **1998**, *109*, 7546–7555.
(51) Arrighi, V.; Higgins, J. S.; Burgess, A. N.; Howells, W. S. *Macromolecules* **1995**, *28*, 2745–2753.
(52) Arrighi, V.; Higgins, J. S. *Physica B* **1996**, *266*, 1–9.
(53) Genix, A.-C.; Arbe, A.; Alvarez, F.; Colmenero, J.; Farago, B.; Wischnewski, A.; Richter, D. *Macromolecules* **2006**, *39*, 6260–6272.
(54) Kuebler, S. C.; Schaefer, D. J.; Boeffel, C.; Pawelzik, U.; Spiess, H. *Macromolecules* **1997**, *30*, 6597–6609.
(55) Bée, M. *Quasielastic Neutron Scattering*; Adam Hilger: Bristol, U.K., 1988.

MA802183H